Composites Science and Technology xxx (xxxx) xxx-xxx

Contents lists available at ScienceDirect

Composites Science and Technology

journal homepage: http://ees.elsevier.com

Nanocomposites with size-controlled nickel nanoparticles supported on multi-walled carbon nanotubes for efficient frequency-selective microwave absorption

Francisco Mederos-Henry [a,c], Sébastien Depaifve [a,1], Arnaud Wolf [a,1], Yann Danlée [b,c], Arnaud Delcorte [b], Christian Bailly [b], Isabelle Huynen [c,**], Sophie Hermans [a,*]

[a] Institute of Condensed Matter and Nanosciences (IMCN), Division of Molecules, Solids and Reactivity (MOST), Place Louis Pasteur 1, Université Catholique de Louvain, Louvain-la-Neuve, B-1348, Belgium

[b] Institute of Condensed Matter and Nanosciences (IMCN), Division of Bio and Soft Matter (BSMA), Croix du Sud 1, Université Catholique de Louvain, Louvain-la-Neuve, B-1348, Belgium

[c] Institute of Information and Communication Technologies, Electronics and Applied Mathematics (ICTEAM), Place du Levant 3, Université Catholique de Louvain, Louvain-la-Neuve, B-1348, Belgium

ARTICLE INFO

Keywords
A. Carbon nanotubes
A. Nanocomposites
A. Nanoparticles B. magnetic properties electromagnetic bandgap control

ABSTRACT

Two types of nanocomposites based on multiwalled carbon nanotubes (MWCNTs) decorated with metallic nickel nanoparticles (NiNPs) possessing very different size distributions (13 vs. 130 nm) were produced using novel synthetic techniques. The obtained nanocomposites were dispersed in a polycarbonate (PC) matrix to produce thin (~500 μm) composite films. For the first time, we show that such films possess clear ferromagnetic resonances in the ultra-high frequency (UHF) and L microwave regions. Furthermore, we prove that their natural ferromagnetic (FMR) frequency is lowered when using nanocomposites with smaller NiNPs. These results could be exploited to design selective dual-band filters for telecommunications applications.

1. Introduction

Wireless data communication *via* electromagnetic (EM) transmission in the microwave range is ubiquitous. Mobile and cordless phones, phone mast antennas, Wi-Fi, WLAN and Bluetooth are some examples of telecommunication modes that have carried wave frequencies within the GHz-band. The extensive use of these media in everyday life has led to growing concern about EM interference (EMI). The interference issue can occur between different devices, amongst subcomponents of sensitive devices themselves or within the power microchips [1]. Furthermore, the current communication apparatus must support multiple radio frequency bands; the mobile phone is so far the most common example with a tri-band, quad-band or penta-band embedded system [2]. This multiplication of narrow frequency bands is extremely complex because of massive and entangled signal transmission and reception. Besides, in the last decade, the so-called electromagnetic hypersensitivity (EHS) disorder has attracted global attention given its potential consequences on public health. Unfortunately, no precise scientific basis has yet been given to this phenomenon [3] and the debate about the health risks posed by EMs continues to rage.

The classical EMI shielding solution is based on EM reflectors such as metal foils or coatings [4]. However, these methods are considered more and more unsatisfactory given that they simply deflect the unwanted EM signal, shifting the problem elsewhere. Broadband absorption becomes the unique convincing solution in various circumstances (*e.g.* dysfunction of microchips, disturbed signal transmission, EM pollution or EHS disorder) as it completely removes the disruptive EM waves. However, new sophisticated devices require smart management of absorption in specific bands. Indeed, multi-band telecommunications are already essential for many usual devices. Where the bands are widely separated in frequency, parallel transmit and receive signal path circuits must be provided, which increase the cost, complexity and power demand of such multi-band devices [5].

The electromagnetic bandgap (EBG) concept is a simple solution for such a control or filtering system. It consists of creating a low transmission (ideally null) in one or more frequency bands. However, common GHz-EBG solutions are intrinsically complex and expensive [6]. The EBG manufacturing methods are thus limited to very specific applications [7]. The solution proposed in this work uses intrinsic EM properties of materials to absorb a specific frequency band. The composite that we now report offers frequency-selective absorption depending on the size of the synthesized nanoparticles, which is of prime interest for dual band operating communication systems.

We have already reported on microwave absorbers based solely on conductive nanocarbon supports (NcS) dispersed in a polycarbonate (PC) matrix [8–10]. We are now developing a new generation of highly efficient, thin microwave absorbers built from three main blocks [11]. The first one is a highly conductive NcS such as multi-walled carbon nanotubes (MWCNTs) or graphene nanoplatelets (GNPs). The second consists of different types of ferro- or ferri-magnetic nanoparticles (MNPs). Indeed, MNPs show a ferromagnetic resonance (FMR) in the microwave range, an intense absorption event that can be exploited to enhance signal absorption [12,13]. These first two build-

* Corresponding author.
** Corresponding author.
E-mail addresses: isabelle.huynen@uclouvain.be (I. Huynen); Sophie.Hermans@uclouvain.be (S. Hermans)
[1] Present address: Materials Research and Technology Department (MRT), Luxembourg Institute of Science and Technology (LIST), Hautcharage L-4940, Luxembourg.

https://doi.org/10.1016/j.compscitech.2019.107947

ing blocks are brought together by decorating the NcS with such MNPs. In a consecutive step, they are dispersed in the third element of our system, a host polymeric matrix. The final composite will therefore possess all the properties of polymer materials, *i.e.* flexibility, conformability, moldability, mechanical strength etc., allowing shaping of the absorber by classical polymer processing techniques.

Different strategies have been used to create composite materials based on the dispersion of a ferromagnetic component in a polymer matrix. The most common examples address the dispersion of either magnetic nanowires [14] or nanocomposites consisting of magnetic nanoparticles (MNP) grafted on carbonaceous nanostructures [15] or trapped inside CNTs [16,17], as well as hybrid structures mixing MNPs and CNTs [18,19]. Magnetic nanowires impart high ferromagnetic behavior to the end composite material. However, the large-scale production of nanowires is unrealistic. Grafted or trapped MNPs on/in CNTs seems more adapted for medium-scale production and they lead to the highest magnetization/mass ratio.

In the present study, the microwave absorption properties of novel micrometric films composed of MWCNTs solvothermally decorated with nickel nanoparticles (NiNPs) and dispersed in PC are shown for the first time. Here, we demonstrate that such films possess a clear ferromagnetic resonance (FMR) response in the ultra-high frequency (UHF) band (0.30–1 GHz) and the L-band (1–2 GHz) and that their natural FMR frequency depends on the size of the deposited NiNPs. These results could be implemented in telecommunication applications to design a passive micrometric EBG filter showing selective dual band absorption.

2. Materials and methods

2.1. Materials

NC3100 MWCNTs (95%C purity) were obtained from Nanocyl (Belgium). All other reagents were supplied by Bayer Material Science, Alfa Aesar or VWR and used as received. More details on each reagent are provided in the Supplementary Material (SM).

2.2. Solvothermal synthesis and thermal annealing of the Ni@MWCNTs nanocomposites

Two solvothermal methods were developed to produce Ni@MWCNTs nanocomposites with different NiNPs size distributions. The first was carried out at ambient pressure (abbreviated AP) while the other was performed in an autoclave (abbreviated AC). After synthesis, both products were thermally annealed in order to promote further particle growth by sintering. Detailed information on the synthetic procedures can be found in the Supplementary Material, section 2.

2.3. Ni@MWCNTs nanocomposites dispersion in a polycarbonate (PC) matrix (Ni@MWCNTs_PC)

The thermally-annealed AP and AC Ni@MWCNTs nanocomposites produced with a 0.8 mM PVP concentration were dispersed in polycarbonate (PC) using the melt-mixing methodology described in Ref. [13]. PC was dried under vacuum at 70 °C for 24 h before melt compounding. The quantities of each Ni@MWCNTs product and PC were calculated to produce a composite containing 2% (w/w) of MWCNTs. Given that each synthetic technique produced different NiNPs loading rates (abbreviated to Ni/C %LRs), the Ni@MWCNTs and PC quantities are slightly different in each case (see Table 1).

Table 1
Ni@MWCNTs and polycarbonate (PC) quantities engaged for production of the Ni@MWCNTs_PC composites considering the different NiNPs loading rates (Ni/C % LR).

Ni@MWCNTs nanocomposite	Ni/C % LR (%)	Ni@MWCNTs (mg)	PC (g)
AP	21	300	11.7
AC	28	375	11.6

Ni@MWCNTs_PC samples were produced by introducing Ni@MWCNTs and dried PC powders in a co-rotating twin-screw DSM-15 micro-extruder preheated at 250 °C. The mixture was melt-mixed at that temperature for 10 min and 250 rpm. It was then extruded through a 0.5 mm-diameter die, resulting in an output filament of the same average diameter. The filament was left to cool down to ambient temperature. It was then immediately cut into pellets less than 1 cm in length for production of Ni@MWCNTs_PC films.

2.4. Film formation by compression molding

Ni@MWCNTs_PC films were produced by compression molding. In a typical procedure, 2.5 g of the Ni@MWCNTs_PC filament pellets were evenly distributed at the center of a mold placed on top of a Tisoflon® (from Isoflon) PTFE sheet. The mold was a square frame cut in a 0.5 mm-thick steel plate. A second Tisoflon® sheet was then placed on top, so that the material was squeezed between two antiadhesive layers. Two steel plates where then placed beneath and above the sandwiched structure.

The whole set-up was transferred into a Fontijne hot press (Fontijne Grotnes Group, Netherlands), preheated at 250 °C. Starting at t_o (see Fig. 1), the sample was left to melt during 30 s (up to t_1). After t_1, the pressure was increased to 2.5 T and immediately released. This action was repeated for 15 s (t_1 to t_2), increasing the applied pressure in each cycle to remove trapped air bubbles. The pressure was then raised and kept at 10 T for 1 min and 45 s (t_2 to t_3), summing up to a total compression molding time of about 2 min.

The samples were next transferred to a cold Fontijne press and compressed at 7.5 T for 2 additional minutes (t_4 to t_5). The sandwiched structure was then removed, carefully peeling the Teflon sheets to recover the Ni@MWCNTs_PC film.

2.5. Characterization

Powder X-ray diffraction (XRD). Ni@MWCNT powder samples were introduced into 0.5 mm thin-walled glass capillaries (Hilgenberg GmbH, Germany), mounted on a goniometer head and kept at 200 mm distance from the detector. Diffractograms were then collected at room temperature using a MAR345 diffractometer (MarResearch GmbH), a Mo-Kα (0.71073 Å) anode and a XENOCS focusing mirror. The obtained 2D diffractograms were azimuthally integrated using the Fit2D software, calibrated with a LaB_6 standard (NIST 660b Standard).

Scattering matrix (S-parameters) measurements. Electromagnetic (EM) characterization of the Ni@MWCNT_PC films was performed using the microstrip method as described in Ref. [20]. Measurements were performed with an Agilent N5245A PNA-X 70 GHz vector network analyzer (VNA). A DC magnetic field was applied perpendicularly using a NTM 10400M-260 electromagnet. Data acquisition was performed using Labview and the obtained measurements were treated to remove spurious losses induced by connectors and substrate as well as losses induced by the conductive CNTs. As a result, the magnetic response of the film is isolated and presented in the paper. More details on sample preparation, the experimental setup and data treatment is given in the Supplementary Material, Sections 1 and 5.

Superconducting Quantum Interference Device (SQUID) magnetometer. Magnetization measurements of the Ni@MWCNT powders were performed using a Quantum Design MPMS-XL5 SQUID magnetometer with-

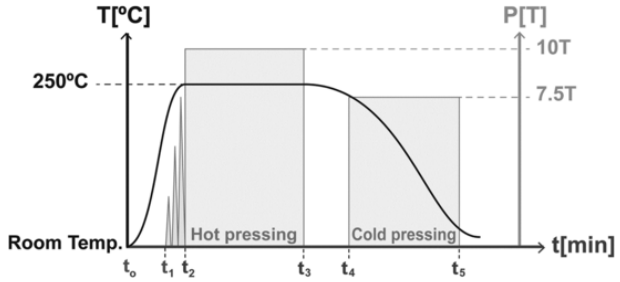

Fig. 1. Schematic representation of the compression molding procedure.

out any further sample preparation. Magnetization curves as a function of an applied magnetic field, *M(H)*, were measured at 300 K after applying a subsequent degaussing procedure. The magnetization was then measured at constant temperature by sweeping the magnetic field from +7 T to −7 T, and then from −7 T to +7 T. Temperature dependent magnetization *M(T)* curves were recorded as follows: the sample was introduced in the SQUID at room temperature and cooled down to 4 K with no applied field (zero-field-cooled (ZFC) curve) after applying a careful degaussing procedure. A magnetic field of 40 mT was applied, and the *M(T)* curve was recorded upon heating from 4 to 295 K. The sample was then cooled down to 5 K under the same applied field (field-cooled curve).

Transmission electron microscopy (TEM). Samples were dispersed in hexane by sonication. Three drops of the supernatant were then deposited onto a holey carbon film supported on a copper grid (C-flat, Protochips, USA), and left to dry, overnight, at room temperature under vacuum. TEM images were obtained on a LEO 922 OMEGA Energy Filter Transmission Electron Microscope operating at 120 kV. Measurements of particle size were executed with the AnalySIS Auto 5.0 software (Olympus Soft Imaging Solutions GmbH, Germany) on at least 100 particles per sample as recorded on the TEM images.

Thermogravimetric analysis (TGA). Ni@MWCNTs powder samples (5–10 mg) were placed in alumina crucibles and introduced in a Mettler Toledo TGA/SDTA 851e instrument. Thermograms were recorded up to 900 °C using a 10 °C/min heating rate under air flux. The samples were recovered after heating and analyzed by XRD as described above, identifying in all cases a NiO phase. TGA data treatment required for the calculation of the Ni/C loading rates was based on the formula weight of this nickel oxide phase. Corrections for residual non-carbonaceous impurities present in MWCNTs were also included in these calculations.

Vibrating sample magnetometer (VSM). The magnetization measurements of the Ni@MWCNTs_PC films were performed with a VSM apparatus (Oxford Instruments) at room temperature using typical sweep rates between 0.06 and 0.12 T/min. The magnetic field was applied to the sample in a perpendicular direction at all times. The obtained results were normalized with respect to the amount of NiNPs contained in each film. To do so, the corresponding Ni/C %LR values determined by TGA analysis were used.

X-Ray photoelectron spectroscopy (XPS). A few milligrams of each sample were deposited on a double-sided adhesive tape attached to a brass cup, and then introduced onto a Macor® carousel. The analyses were performed on a SSX 100/206 photoelectron spectrometer from Surface Science Instruments (USA) equipped with a monochromatized micro focused Al X-ray source (powered at 20 mA and 10 kV). The pressure in the analysis chamber was around 10^{-6} Pa. A flood gun set at 8 eV and a Ni grid placed 3 mm above the sample surface were used for charge stabilization. The C-(C,H) component of the carbon C1s peak was fixed to 284.8 eV to set the binding energy scale. Data treatment was performed with the CasaXPS program (Casa Software Ltd, UK). Spectra were decomposed with the least squares fitting routine provided by the software with a Gaussian/Lorentzian (85/15) product function and after subtraction of a Shirley-type baseline [21]. Molar fractions were calculated using peak areas normalized on the basis of acquisition parameters and sensitivity factors provided by the manufacturer.

3. Results and discussion

The aim of the present study is to characterize the microwave absorption properties of thin films composed of Ni@MWCNTs nanocomposites dispersed in a polycarbonate (PC) matrix. We also explored the impact of NiNPs sizes on the microwave absorption properties of these materials, particularly on their natural FMR frequency (ferromagnetic resonance at zero external magnetic field). Accordingly, we first developed two novel solvothermal methods to prepare Ni@MWCNT nanocomposites with different NiNP size distributions. Afterwards, the nanocomposite powders were dispersed in PC. The obtained Ni@MWCNTs_PC composite materials were hot-pressed to create thin films (~500 μm). VSM and VNA-based scattering matrix measurements were performed on these films to determine their magnetic as well as their microwave absorption properties. The obtained results were also com-

3.1. Characterization of the synthesized Ni@MWCNT nanocomposites

The two synthesized Ni@MWCNT nanocomposites were thoroughly characterized to determine the NiNP purity, loading rate, morphology, size and spatial distribution over the MWCNT surface.

TEM investigation of both nanocomposites after thermal annealing revealed that the deposited NPs possessed strikingly different size distributions. As shown in Fig. 2, the NPs found in the AP product were ten-fold smaller than those found in the AC product (13 vs. 130 nm on average).

Both the AP and AC NPs were found to be composed of a pure face-centered cubic (Ni-fcc) crystalline phase by XRD. Nonetheless, as shown in Fig. 3, additional diffraction peaks of weaker intensity were observed around 19°, 21.5° and 27.8° 2θ angles in the AP diffractogram. Recently, these reflections have been attributed to a nickel carbide phase by Su et al. [22]. They have shown that such metallic carbide phases can form if a NiNP surrounded by a carbon-rich layer is exposed to high temperatures, as an intermediate product of the pyrolysis process. Thus, this minority phase was possibly formed as the employed PVP-10,000 capping agent chains, surrounding the NiNPs, decomposed during thermal annealing. Finally, the reflection observed around $2\theta = 12°$ in both products has been attributed to the ordered arrangement of the concentric cylinders of graphitic carbon in the MWCNTs [23].

XPS analysis of the two nanocomposites after thermal annealing also confirmed the presence of metallic nickel (Ni^0) (see Fig. 4). However, oxidized nickel species (Niox + Niox_sat) were also detected. Their relatively high concentration might be explained by the fact that XPS is a surface analysis technique [24]. Thus, if the oxide is to be found on the surface of the NP, as a passivation layer, the relative amount of the Niox + Niox_sat components will be enhanced relative to that of Ni^0 present in the core. Furthermore, the calculated relative concentrations of each species suggest that the oxide passivation layer is thicker in the AC nanocomposite. In any case, the fact that no oxidized nickel was detected by XRD suggests it is either poorly crystalline or amorphous

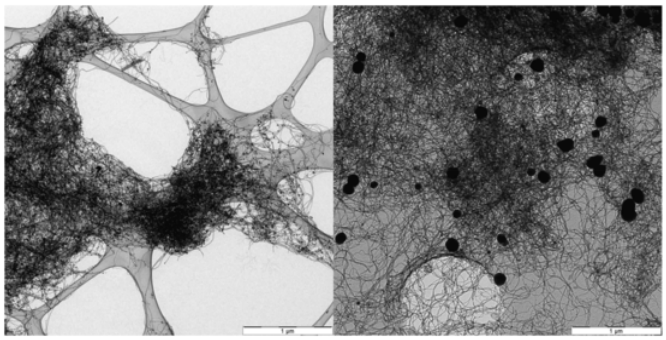

Fig. 2. TEM images showing the thermally annealed AP (left) and AC (right) Ni@MWCNTs nanocomposites synthesized using a 0.8 mM PVP-10,000 concentration.

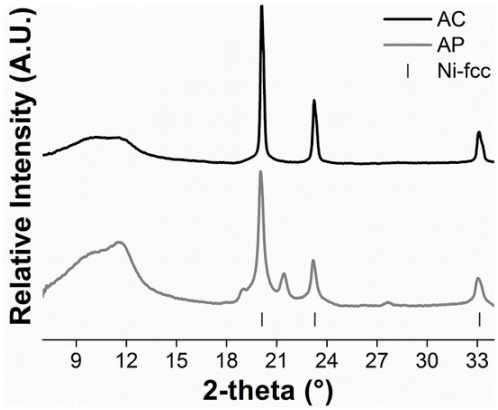

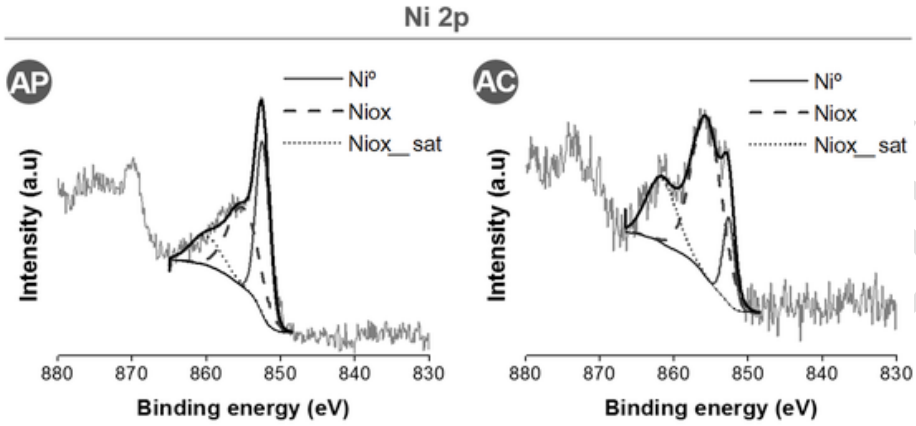

Relative concentration (%)		
Sample	Niº	Niox + Niox_sat
AP	41	59
AC	13	87

Fig. 4. XPS spectra of the Ni 2p peak for the thermally annealed AP (left) and AC (right) Ni@MWCNT nanocomposites synthesized using a 0.8 mM PVP-10,000 concentration. The Ni 2p3/2 peak has been fitted with three components corresponding to metallic (Niº) and oxidized (Niox + Niox-sat) nickel.

in both products. Further characterization information for both nanopowders can be found in the Supplementary Material, Section 3.

3.2. Magnetic properties of the Ni@MWCNTs nanocomposites and their polycarbonate films

The magnetic properties of the thermally annealed Ni@MWCNTs AC and AP nanocomposite powders synthesized with a 0.8 mM PVP concentration were studied by SQUID magnetometry. Their magnetization curves recorded against magnetic field are shown in Fig. 5. As can be observed, significant differences were found in their mass saturation magnetization (M_s), intrinsic coercivity (H_{ci}) and remanent magnetization (M_r) values. While the AC nanocomposite attained an M_s value similar to that of bulk Ni (~55 emu/g), the AP nanocomposite reached only 40 emu/g. Also, the inset of Fig. 2 shows that the AC product possesses H_{ci} and M_r values of ~100 Oe and ~5 emu/g, respectively, while in the AP nanocomposite they are practically zero. These results suggest that the NiNPs in the AC product are ferromagnetic while those in the AP nanocomposite are superparamagnetic, with a blocking temperature (T_B) close to 275 K (see Field and zero-field magnetization against temperature [M(T)] curves, Fig. S12 in the Supplementary Material).

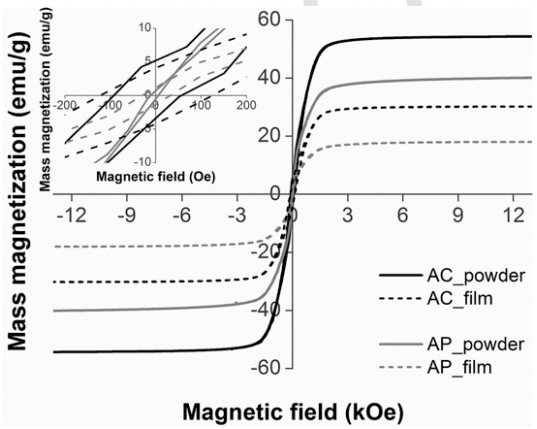

Fig. 5. Magnetization curves recorded against magnetic field at 295 K for the thermally annealed AP and AC Ni@MWCNTs nanocomposite powders synthesized using a 0.8 mM PVP concentration (solid lines) and their corresponding PC films (dotted lines). A detail of the curves (inset, top left) highlights the difference in H_{ci} values of these materials.

These remarkable differences are certainly due to the different sizes of the NiNPs found in each nanocomposite. Superparamagnetic NPs have low M_s and H_{ci} values at room temperature because thermal excitations are sufficient to produce rapid magnetic spin reversals [25,26]. However, in the case of the NiNPs found in the AC nanocomposite, all spins within a single domain are expected to be collinear and rotate in unison due to short-range exchange interactions that minimize the NPs magnetic energy [26]. This stronger magnetic ordering increases the M_s value. Also, higher external field strengths are needed to reverse the direction of the collinear spins found within a single domain, producing a higher H_{ci}. Furthermore, the hysteresis curve of the AC powder denotes the presence of an exchange bias (EB), resulting from the pinning of interfacial spins in the AFM nickel oxide shell to the ones of the FM metallic nickel core. EB coupling results in extra magnetic anisotropy energy, which can also increase the H_{ci} [27].

The magnetic properties of the AP and AC Ni@MWCNT_PC films were characterized using a VSM (see Fig. 5, dotted lines). The most striking feature is that, compared to the nanocomposite powders, the M_s values for both films halved, suggesting that the NiNPs undergo thermal oxidation in the polycarbonate matrix during melt mixing and compression molding. The oxidation of the metallic nickel core reduces the NPs magnetic content, hence reducing their magnetization. As for the H_{ci} and M_r values, the hysteresis curves show that the former magnetic property slightly increases in both films while the latter remains practically unchanged, as compared to their nanopowder counterparts.

3.3. Microwave absorption properties of the Ni@MWCNT_PC films

We characterized the electromagnetic (EM) behavior of both Ni@MWCNT_PC films in the microwave range by measuring their scattering matrix and analyzing the different scattering parameter values.

Fig. 6 shows the results for the S21 transmission parameter of the composite films. As can be observed, a series of absorption processes were recorded, occurring even in the absence of an external applied magnetic field. Also, their frequency shifted towards higher values as the external magnetic field was increased.

These experimental observations indicate that a ferromagnetic resonance (FMR) is occurring in the range of the microwave frequencies under study (40 MHz–20 GHz). FMR is a well-known absorption phenomenon that analogues the paramagnetic and nuclear resonance absorption processes. For

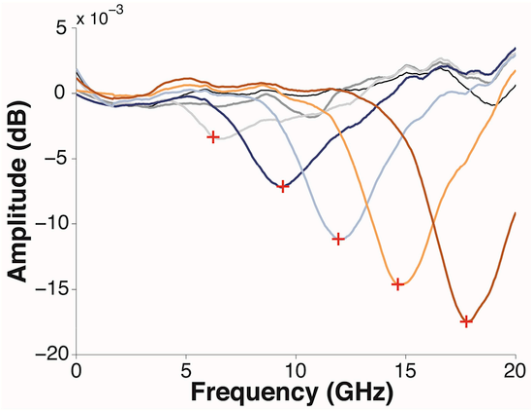

Fig. 6. Typical FMR behavior observed in S21 transmission for the Ni@MWCNTs_PC AP composite film. Red crosses indicate absorption frequency minima. (For interpretation of the references to colour in this figure legend, the reader is referred to the Web version of this article.)

other nanocomposite materials, we have already shown that it can be exploited for the absorption of electromagnetic waves in the microwave range [28].

According to Kittel [29], the resonance frequency of a ferromagnetic material is dependent on the strength of an applied static magnetic field, H_z. Furthermore, if the deposited NPs are large enough to ensure a magnetic moment stability-lifetime, τ, superior to 10^{-9} s [30], an effective anisotropy field (H_a) involving the saturation magnetization is induced in the sample. Under these conditions, a so-called natural resonance can be observed at zero static field ($H_z = 0$). Thus, in perfect agreement with our experimental observations, the Kittel FMR theory predicts the existence of a natural resonance, at zero magnetic field, that tends to shift toward higher frequencies as H_z is increased.

As also shown in Fig. 6, the absorption frequency, f, at each value of applied magnetic field, H_z, was measured by identifying the absorption minima in the S21 curves. Fig. 7 shows the extracted f values for both nanocomposite films plotted as a function of H_z and the linear regressions derived therefrom. The linear dependence of FMR on applied magnetic field was introduced by Kittel [29] and has been observed ever since for a wide range of ferromagnetic and ferrite structures [31–33]. As detailed in the Supplementary Material, the linear regression can be expressed as $f_{FMR} = \gamma(H_z + M_s)$, where γ is the gyromagnetic ratio, determined by the composition of the ferromagnetic NPs. Thus, in agreement with the FMR theory, the AC film, possessing a higher M_s, exhibits a higher natural FMR frequency (1.12 GHz) than the AP film (0.68 GHz). This relatively small difference in natural resonance frequency is significant considering the high precision of our EM characterization setup (see Supplementary Material, Sections 1 and 5). They cannot be attributed to the MWCNTs, since they have no global magnetic response [34,35]. They can neither be attributed to the amount of loaded NiNPs given that the Ni/C %LR is very similar for both nanocomposites (see Table 1). Also, as shown in Fig. 7, the gyromagnetic ratios of the films are close (within 2.2% difference), thus indicating similarity in the composition of the dispersed AP and AC NiNPs. As shown in the Supplementary Material, Section 5, the difference originates from the different saturation magnetization values of the AP and AC samples, resulting from different NiNPs size distributions, which produce different M_s values. In other words, these results illustrate how variations in the NPs size induce a shift in the composite films natural FMR frequencies. To the best of our knowledge, this is the first time that such an effect is shown for this type of materials.

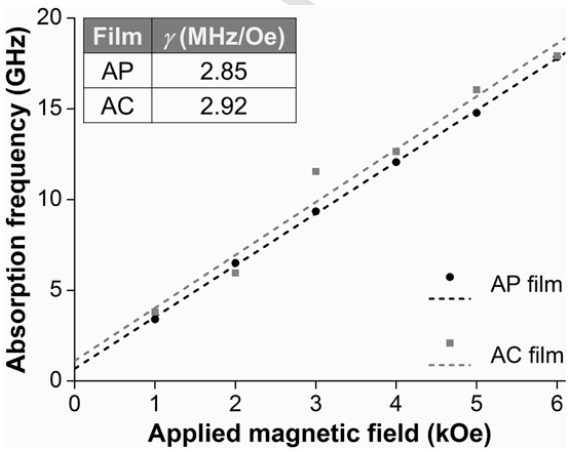

As these results show, the AP and AC films absorb in the UHF-band and L-band respectively which is nowadays exploited for all satellite navigation or cellular phone telecommunication systems. Consequently, the significant difference observed in the natural resonance of both materials could be exploited to design selective dual-band filters for this frequency region.

4. Conclusions

We developed two novel solvothermal methods to decorate multiwalled carbon nanotubes with metallic nickel nanoparticles. The synthetic procedures, followed by thermal annealing, allowed the production of NiNPs with very different size distributions. In the case of the ambient pressure (AP) synthesis, the slow addition of the nickel precursor allowed the deposition of small (13.6 ± 4.4 nm) superparamagnetic NiNPs. In the autoclave (AC) synthesis, much larger (130 ± 47 nm) weakly ferromagnetic NiNPs were obtained. In the latter case, we also proved that we could control their growth by employing different concentrations of polyvinylpyrrolidone (PVP, M.W.10,000) as a capping agent, obtaining slightly smaller NiNPs at higher PVP concentrations.

In both methodologies, NiNPs were found to be composed of a crystalline metallic core surrounded by an amorphous oxidized nickel layer. However, in the AP products, it was also found that PVP thermal decomposition induced the formation of a crystalline nickel carbide phase and a surrounding, possibly graphitic, shell layer.

The obtained nanocomposites were dispersed in a polycarbonate (PC) matrix to produce ultrathin composite films. For the first time, we showed that such films possess a clear ferromagnetic resonance response in the UHF- or L-band. Moreover, our results suggest that their natural FMR frequency can be lowered if the dispersed nanocomposite NiNPs are smaller. The fact that we can tune the absorption frequency of the films by employing nanocomposites with different NiNPs size distributions could be exploited to design selective dual-band filters for telecommunications applications.

CRediT authorship contribution statement

Francisco Mederos-Henry: Conceptualization, Methodology, Software, Validation, Investigation, Writing - original draft, Visualization. **Sébastien Depaifve:** Investigation. **Arnaud Wolf:** Investigation. **Yann Danlée:** Methodology. **Arnaud Delcorte:** Resources, Writing - review & editing, Funding acquisition. **Christian Bailly:** Methodology. **Isabelle Huynen:** Conceptualization, Methodology, Software, Resources, Writing - review & editing, Supervision. **Sophie Hermans:** Conceptualization, Methodology, Resources, Writing - original draft, Writing - review & editing, Supervision, Project administration, Funding acquisition.

Declaration of competing interest

The authors declare that they have no known competing financial interests or personal relationships that could have appeared to influence the work reported in this paper.

Acknowledgements

This work is supported by the Communauté Française de Belgique, through the project "Nano4waves" funded by its research program "Actions de

tory) and Dr. Yinguo Xiao (Forschungszentrum Jülich) for their help with SQUID measurements as well as Dr. Sergei Basov (Université catholique de Louvain-BSMA) and Pascal Simon (Université catholique de Louvain - WELCOME technological platform) for their support while performing the VSM and VNA measurements. Warm thanks also go to R. A. Layfield for proofreading the manuscript.

Appendix A. Supplementary data

Supplementary data to this article can be found online at https://doi.org/10.1016/j.compscitech.2019.107947.

References

[1] N. Violette, Electromagnetic Compatibility Handbook, Springer Netherlands, Amsterdam, 1987.
[2] A. Benslimane, H. Tobiet, QoS classification for mobile networks: international roaming case study, In 5th IEEE International Conference on High Speed Networks and Multimedia Communication, Jeju Island, South Korea, 2002.
[3] Scientific Committee on Emerging and Newly Identified Health Risks, Opinion On Potential Health Effects of Exposure to Electromagnetic Fields (EMF) [Online], European Comission, 2015. https://ec.europa.eu/health/sites/health/files/scientific_committees/emerging/docs/scenihr_o_041.pdf.
[4] Leland H. Hemming, Architectural Electromagnetic Shielding Handbook: A Design and Specification Guide, IEEE Press, Piscataway: NJ, USA, 2000.
[5] Patents US7057472B2 "Bypass Filter, Multi-Band Antenna Switch Circuit, and Layered Module Composite Part and Communication Device Using Them" and US6975834B1 "Multi-Band Wireless Communication Device and Method".
[6] N. Engheta, R.W. Ziolkowski, Metamaterials: Physics and Engineering Explorations, John Wiley & Sons & IEEE Press, USA, 2006.
[7] F. Bilotti, L. Vegni, F. Viviani, On EBG structures for cellular phone applications, AEU-Int. J. Electron. C. 57 (6) (2003) 403–408.
[8] Y. Danlée, I. Huynen, C. Bailly, Thin smart multilayer microwave absorber based on hybrid structure of polymer and carbon nanotubes, Appl. Phys. Lett. 100 (2012) 213105.
[9] Y. Danlée, I. Huynen, C. Bailly, Thin and flexible multilayer polymer composite structures for effective control of microwave electromagnetic absorption, Compos. Sci. Technol. 100 (2014) 182–188.
[10] H.M. Mesfin, A.C. Baudoin, S. Hermans, A. Delcorte, I. Huynen, C. Bailly, Frequency selective microwave absorption induced by controlled orientation of graphene-like nanoplatelets in thin polymer films, Appl. Phys. Lett. 105 (2014) 103105.
[11] Y. Danlée, R. Jaiswar, F. Mederos Henry, H. Mesfin, C. Bailly, A. Delcorte, S. Hermans, I. Huynen, Nano4Waves: a metamaterial approach towards smart nanocomposites for nanosecond signal control, IEEE Nano 2015 (15th International Conference on Nanotechnology), 2015 Rome, Italy.
[12] J.V.I. Timonen, R.H.A. Ras, O. Ikkala, M. Oksanen, E. Seppälä, K. Chalapat, J. Li, G.S. Paraoanu, Magnetic nanocomposites at microwave frequencies, in: A. Aldea, V. Bârsan (Eds.), Trends in Nanophysics: Theory, Experiment And, Technology, Springer Science, London, United Kingdom, 2010, pp. 257–285.
[13] L.B. Kong, L. Liu, Z. Yang, S. Li, T. Zhang, in: Y. Hou, D.J. Sellmyer (Eds.), Magnetic Materials for Electromagnetic Wave Absorption" in Magnetic Nanomaterials: Fundamentals, Synthesis and Applications, Wiley-VCH Verlag GmbH & Co., Weinheim, Germany, 2017, pp. 473–514.
[14] Y. Li, X.F. Yin, F.R. Chen, H.H. Yang, Z.X. Zhuang, X.R. Wang, Synthesis of magnetic molecularly imprinted polymer nanowires using a nanoporous alumina template, Macromolecules 39 (13) (2006) 4497–4499.
[15] X. Pei, Y.H. Yan, L. Yan, P. Yang, J. Wang, R. Xu, M.B. Chan-Park, A magnetically responsive material of single-walled carbon nanotubes functionalized with magnetic ionic liquid, Carbon 48 (9) (2010) 2501–2505.
[16] R.K. Srivastava, T.N. Narayanan, A.P. Reena Mary, M.R. Anantharaman, A. Srivastava, R. Vajtai, P.M. Ajayan, Ni filled flexible multi-walled carbon nanotube–polystyrene composite films as efficient microwave absorbers, Appl. Phys. Lett. 99 (2011) 113116.
[17] A. Leonhardt, M. Ritschel, D. Elefant, N. Mattern, K. Biedermann, S. Hampel, C.H. Müller, T. Gemming, B. Büchner, Enhanced magnetism in Fe-filled carbon nanotubes produced by pyrolysis of ferrocene, J. Appl. Phys. 98 (7) (2005) 074315.
[18] Z. Zheng, B. Xu, L. Huang, L. He, X. Ni, Novel composite of Co/carbon nanotubes: synthesis, magnetism and microwave absorption properties, Solid State Sci. 10 (3) (2008) 316–320.
[19] Y.R. Jang, J.I. Lee, Magnetism of linear Fe, Co, and Ni nanowires encapsulated in zigzag (n, 0) carbon nanotubes (CNT) with n = 5 to 9: a first-principles study, Phys. Status Solidi B 244 (12) (2007) 4407–4410.
[20] N. Quiévy, P. Bollen, J.-M. Thomassin, C. Detrembleur, T. Pardoen, C. Bailly, I. Huynen, Electromagnetic absorption properties of carbon nanotube nanocomposite foam filling honeycomb waveguide structures, IEEE Trans. Electromagn Compat. 54 (2012) 43–51.
[21] D.A. Shirley, High-resolution X-ray photoemission spectrum of the valence bands of gold, Phys. Rev. B5 (1972) 4709–4714.
[22] Y. Su, C. Chen, X. Zhu, Y. Zhang, W. Gong, H. Zhang, H. Zhao, G. Wang, Carbon-embedded Ni nanocatalysts derived from MOFs by a sacrificial template method for efficient hydrogenation of furfural to tetrahydrofurfuryl alcohol, Dalton Trans. 46 (2017) 6358–6365.
[23] Y. Zhang, S. Xiao, Q. Wang, S. Liu, Z. Qiao, Z. Chi, J. Xu, J. Economy, Thermally conductive, insulated polyimide nanocomposites by AlO (OH)-coated MWCNTs, J. Mater. Chem. 21 (2011) 14563–14568.
[24] S. Tanuma, C.J. Powell, D.R. Penn, Calculations of electron inelastic mean free paths. IX. Data for 41 elemental solids over the 50 eV to 30 keV range, Surf. Interface Anal. 43 (2011) 689–713.
[25] H.M. Lu, W.T. Zheng, Q. Jiang, Saturation magnetization of ferromagnetic and ferromagnetic nanocrystals at room temperature, J. Phys. D Appl. Phys. 40 (2007) 320–325.
[26] G.C. Papaefthymiou, Nanoparticle magnetism, Nano Today 4 (2009) 438–447.
[27] X. Liu, B.P. Pichon, C. Ulhaq, C. Lefèvre, J.-M. Grenèche, D. Bégin, S. Bégin-Colin, Systematic study of exchange coupling in core–shell $Fe_{3-\delta}O_4$@CoO nanoparticles, Chem. Mater. 27 (2015) 4073–4081.
[28] F. Mederos-Henry, B.P. Pichon, Y. Tchuitio Yagang, A. Delcorte, C. Bailly, I. Huynen, S. Hermans, Decoration of nanocarbon solids with magnetite nanoparticles: towards microwave metamaterial absorbers, J. Mater. Chem. C. 4 (2016) 3290–3303.
[29] C. Kittel, On the theory of ferromagnetic resonance absorption, Phys. Rev. 73 (2) (1948) 155–161.
[30] M. Charilaou, K.K. Sahu, D. Faivre, A. Fischer, I. García-Rubio, A.U. Gehring, Magnetic anisotropy of non-interacting collinear nanocrystal-chains, Appl. Phys. Lett. 99 (2011) 182504.
[31] G. Goglio, S. Pignard, A. Radulescu, L. Piraux, I. Huynen, D. Vanhoenacker, A. Vander Vorst, Microwave properties of metallic nanowires, Appl. Phys. Lett. 75 (12) (1999) 1769–1771.
[32] A. Encinas-Oropesa, M. Demand, L. Piraux, I. Huynen, U. Ebels, Dipolar interactions in arrays of Nickel nanowires studied by ferromagnetic resonance, Phys. Rev. B 63 (2001) 104415.1-6.
[33] F. Mederos-Henry, S. Hermans, I. Huynen, Coplanar waveguide method for microwave and ferromagnetic resonance characterization of nanocarbon powders decorated with magnetic nanoparticles, Microw. Opt. Technol. Lett. 59 (9) (2017) 2330–2335.
[34] O.V. Yazyev, Emergence of magnetism in graphene materials and nanostructures, Rep. Prog. Phys. 73 (5) (2010) 056501.
[35] V. Georgakilas, J.A. Perman, J. Tucek, R. Zboril, Broad family of carbon nanoallotropes: classification, chemistry, and applications of fullerenes, carbon dots, nanotubes, graphene, nanodiamonds, and combined superstructures, Chem. Rev. 115 (11) (2015) 4744–4822.